https://doi.org/10.5194/egusphere-2026-6133
Preprint. Discussion started: 20 November 2026
© Author(s) 2026. CC BY 4.0 License.

A Traceable Single-Setup Procedure for Simultaneous Static and Dynamic Humidity Calibration: Demonstration on a Broad Range of 48 Commercial Low-Cost Sensors

Felix Witt[1,2], Volker Ebert[1,3]

[1]Department of Mechanical Engineering, Institute of Reactive Flows and Diagnostics, Technische Universität Darmstadt, Karolinenplatz 5, 64289 Darmstadt, Germany
[2]Institute of Flight Guidance, Technische Universität Braunschweig, Hermann-Blenk-Str. 27, 38108 Braunschweig, Germany
[3]Physikalisch-Technische Bundesanstalt (PTB), Bundesallee 100, 38116 Braunschweig, Germany

Correspondence to: Volker Ebert (volker.ebert@ptb.de)

Abstract. Low-cost relative humidity sensors (LCrHS) are widely used in science, industry, and consumer applications; however, traceable calibration of individual units and proper dynamic characterization are largely unavailable. This work presents a novel calibration procedure, *MetDyHuCal*, implemented in our *dynH$_2$O* test setup. Our approach enables metrologically traceable, static and dynamic humidity calibration within a single setup and during the same measurement campaign. Our setup is based on two absolute optical hygrometers, *SEALDH-II* and *MANTA-LAH* as primary, SI-traceable references - both utilizing *direct tunable diode laser absorption spectroscopy* (dTDLAS). The proposed setup and procedure were applied to 48 LCrHS (9 models from 8 manufacturers). Static calibrations reveal substantial sensor model-level offsets and non-linearities, highlighting the necessity for individual correction of each sensor. Dynamic characterizations yields response times that deviate by −50 % to +81 % from the manufacturer datasheet values. Furthermore, several LCrHS models exhibit a significant, systematic dependence of the measured response time on the absolute humidity level. Together, these results illustrate large performance spreads between nominally identical LCrHS. The reproducibility of the *MetDyHuCal* procedure was assessed by repeated characterisations of 10 sensors, each measured five times on different days and after being removed and reinstalled in the setup. The reproducibility test for the characteristic time constant τ yielded a median relative standard deviation of 1.0 % (mean 1.3 %). We demonstrate that meaningful, traceable performance figures can be obtained using the proposed standardized procedure. Beyond LCrHS, our approach may also be used to characterize the dynamic behaviour of high-end research instruments, such as *HAI*, our multi-channel dTDLAS on the research aircraft *HALO*.

1 Introduction

Low-cost relative humidity sensors (LCrHS) to measure the relative water content (rH) in gases have become indispensable components across a broad range of scientific fields, and in many important industrial or consumer applications. LCrHS are routinely employed in air-conditioning systems, in industrial process control and monitoring, including fuel cell management, food processing, pharmaceutical production, or drying processes (TE Connectivity, 2017; Nikolaev et al., 2018; E+E Elektronik GmbH, 2022; Santos Jr et al., 2025; Mihajlo et al., 2020). In research, the use cases range from low-cost weather balloon payloads to agricultural monitoring or even low-cost eddy-correlation systems for evapotranspiration measurements (Hooshmand, 2025; Zhang et al., 2014; Macagga et al., 2024; Markwitz and Siebicke, 2019; Sari et al., 2023; Wiyagi et al., 2017). LCrHS are used in even larger quantities in the consumer field, e.g. in weather stations or IoT devices (Gupta et al., 2024; Holovatyy, 2021; Hartono and Utama, 2025; Hossain et al., 2025).

In the context of this work, we define a low-cost hygrometer (LCrHS) via a purchase price of less than 50 € per unit. LCrHS selection is typically driven by cost pressure and the need for availability in quantities of 100-1000s e.g. for sensor networks, to very large quantities, millions, for consumer applications. Other important selection parameters are: Small size, low electrical power consumption, digital readout and communication protocols, as well as seamless integration into the target setup.

https://doi.org/10.5194/egusphere-2026-6133
Preprint. Discussion started: 20 November 2026
© Author(s) 2026. CC BY 4.0 License.

In all the named applications of LCrHS, dynamic humidity changes are to be expected, and the dynamic sensor performance can be influencing the performance of the full measurement system. In applications where the measured humidity is used as input for a control loop (e.g. air conditioning) or where the dynamic changes itself are to be quantified, e.g. industrial process control, weather balloons or scientific eddy-correlation systems, the dynamic response behaviour of the individual LCrHS needs to be understood. The sensor performance as well as its inter-specimen variability need to be accurately specified to choose a LCrHS suitable for the target application.

A traceable characterization of the static performance of the individual sensor type (average and spread) and in particular of the individual sensor is usually missing. Even worse is the availability of performance and calibration data concerning the dynamic LCrHS response. Furthermore, the origin of the characterization data is unclear and influenced by the lack of standardized and widely adopted test procedures as well as the unknown characterization procedures und setups used by the manufacturers. Even worse is the lack of traceability information.

In this work we present the in-depth application of our new test setup (called "dynH_2O") for simultaneous static and dynamic rH-sensor characterisation. Further, we characterize the performance of our novel, static and dynamic calibration method for "Metrological Dynamic Humidity Calibration" = "MetDyHuCal". Finally, we combine our automated setup and test procedure and demonstrate the traceable, automated, static and dynamic calibration of a selection of 48 commonly used LCrHS, originating from 8 manufacturers. The result is a prove of concept for setup and method. Furthermore, we generate the first, comprehensive, traceable, dynamic performance dataset of commonly used LCrHS from different manufacturers using a new, well-defined metrological method.

1.1 State of the Art

The characterization of LCrHS currently can be performed at four levels: User - Manufacturer - calibration service industry - or national metrology institutes (NMI).

At the user level, access to traceable calibration references is often very limited (Koestoer et al., 2019). The use of saturated salt solutions to realize fixed relative humidity values for field calibration is common practice (VDI/VDE 3514 Blatt 3, 2021). However, the dynamic behaviour of a LCrHS is in most cases – if at all - only considered during the sensor selection process and is rarely assessed by the user during calibration or even applied to correct dynamic measurements.

At the manufacturer level, a single, so-called "group calibration function" is applied as a unified "description" of all individual sensors of a given model. Metrological calibration of individual sensors is very rare, due to the associated cost. Individual sensor calibration is - in some cases - offered on user request by the manufacturer or by external calibration services. However, the associated characterisation costs are significantly higher than the sensor purchase price.

The dynamic LCrHS response is typically characterised only once during the initial test phase of the sensor model and is subsequently reported in the datasheet, as the T_{63} or τ time constant. The constant describes the time the sensor needs to reach 63 % of the final concentration after an "infinitely" steep humidity step change. Stating a single τ value requires, that the sensor response can be described with a first-order low-pass model. Only then, the τ value remains constant and independent of the start and end value of the humidity step change (Liptak, 2005).

The dynamic characterisation of individual sensors is - to our knowledge - not offered by any commercial calibration laboratory due to even higher cost and time requirements. Furthermore, there is very little to no information given to the user on the traceability path of the characterisation setup used by the manufacturers.

At the level of national metrology institutes (NMI), the current state-of-the-art consists of static multi-point calibrations performed in gas-flow climate chambers, employing primary or secondary two-pressure humidity generators as humidity reference sources (Wettstein and Mutter, 2018) as evidenced by key comparisons of the Consultative Committee for Thermometry (CCT), like CCT-K6, which evaluates the realization of local dew-point temperature scales in in the range −50 °C to +20 °C (Bell et al., 2015). In this approach, the relative humidity of the gas is either calculated from the water vapor

https://doi.org/10.5194/egusphere-2026-6133
Preprint. Discussion started: 20 November 2026
© Author(s) 2026. CC BY 4.0 License.

saturation pressure and the temperature in the saturator, combined with the temperature and pressure in the vicinity of the device under test (DUT) or the reference value is measured close to the DUT using a reference rH analyser (instead of a rH generator). The most common reference analyser principle is the chilled mirror hygrometer (CMH) (Fernicola et al., 2026). Both methods - preparative and analytical - are traceable and able to achieve relative measurement uncertainties between 0.2 and 1.5 % (BIPM, 2026), but are time-consuming and hence costly.

Critically, no certified, metrological Calibration and Measurement Capability (CMC) based calibration service exists at any NMI for the dynamic characterisation of hygrometers. There is no CMC entry for dynamic humidity calibration registered in the global Key Comparison Database (KCDB) of the Bureau International des Poids et Mesures (BIPM) (BIPM, 2026).

1.2 Required improvements from the current state of the art

The current state of the art gives rise to two clearly identifiable problems for LCrHS users:

Problem A, concerns metrological static calibration. LCrHS are typically deployed without individual, traceable calibration. As a result, they carry unknown systematic measurement errors and offsets.

Problem B, concerns the unknown dynamic behaviour of LCrHS. In dynamic measurement environments, LCrHS show systematic amplitude and phase offsets, that are not corrected for (Bärfuss et al., 2023; Bärfuss et al., 2018; Mitter, 2006). When such a sensor is part of a control loop, these uncharacterised dynamic deviations can cause control errors and even instabilities (Wang, 2014). Most real-world applications involve relative humidity that varies dynamically, yet the dynamic response of LCrHS is rarely characterised in any detail and with traceability.

Two problems exist at the fundamental metrological level:

First, to our knowledge no dynamical metrological calibration service is available for users. The topic of dynamic hygrometer calibration has been investigated by national metrology institutes and other research groups in the EURAMET research projects *MeteoMet2*, *HIT* and *MefHySto* (Mitter, 2006; Merlone et al., 2018; Heinonen et al., 2015; Tuma, 2023). However, the results from these studies have so far not led to the implementation of publicly available calibration services.

Second, standardised procedures for dynamic calibration and characterisation are very rare. To date, only one national standard for dynamic humidity calibration exists: The French standard NF X 15-113 (NF X 15-113, 1997).

1.3 Needs of the user

Four complementary user needs motivate the development of the method presented in this paper:

Need A is a setup capable of the traceable preparation of well-defined dynamic water vapour concentration changes (Witt et al., 2023a; Witt et al., 2021a).

Need B is a validated dynamic calibration procedure that can be applied to industrial and low-cost sensors (Witt et al., 2023b; Witt and Ebert, 2023).

Need C, which constitutes the central contribution of this paper, is the demonstration and verification of this dynamic measurement setup, the dynH_2O system, together with the calibration procedure MetDyHuCal, applied to a large set of commercially available LCrHS of different models and from different manufacturers.

Need D is a far-reaching automation of the dynamic calibration measurements and the associated data evaluation, with the aim of minimising both calibration cost and time consumption.

1.4 Benefits for the user

The setup and method presented in this work has two main benefits for LCrHS users: The primary benefit is to get a better understanding of the capabilities and limitations of LCrHS. Further our work provides the ability to get reliable data on the dynamic behaviour of their LCrHS, enabling accurate sensor intercomparisons across different manufacturers. This substantially simplifies the selection of the most appropriate sensor for a given measurement task and enables the assessment,

https://doi.org/10.5194/egusphere-2026-6133
Preprint. Discussion started: 20 November 2026
© Author(s) 2026. CC BY 4.0 License.

quantification and potentially the correction of dynamic measurement errors. Another benefit of our setup is the combination of both dynamic and static calibration within a single unified measurement setup. The overall measurement time of this combined procedure is comparable to that required for a conventional static multipoint calibration alone, while yielding considerably more metrological information about the DUT.

2 Experimental Setup

The MetDyHuCal calibration procedure is implemented in the dynH_2O setup, a novel dedicated metrological stepped-flow facility developed by the authors. The setup is designed to generate fast, well-defined, steps in the water vapor amount fraction at controlled and minimized flow, temperature, and pressure disturbances. The setup simultaneously monitors the generated gas humidity within the flow channel, without requiring any gas sampling process. This is achieved with a temporal resolution of up to 100 Hz, by the gas sampling-free, SI-traceable reference laser spectrometer MANTA-LAH (MultipAth Nonextractive TunAble Laser Absorption Hygrometer). The H_2O amount fraction is measured in µmol per mol (µmol/mol). For simplicity µmol per mol will be referred to as parts per million (ppm).

The pneumatic plan of the full setup is shown in Figure 1. The CAD rendering, including a cut-through view of the flow section, is shown in Figure 2.

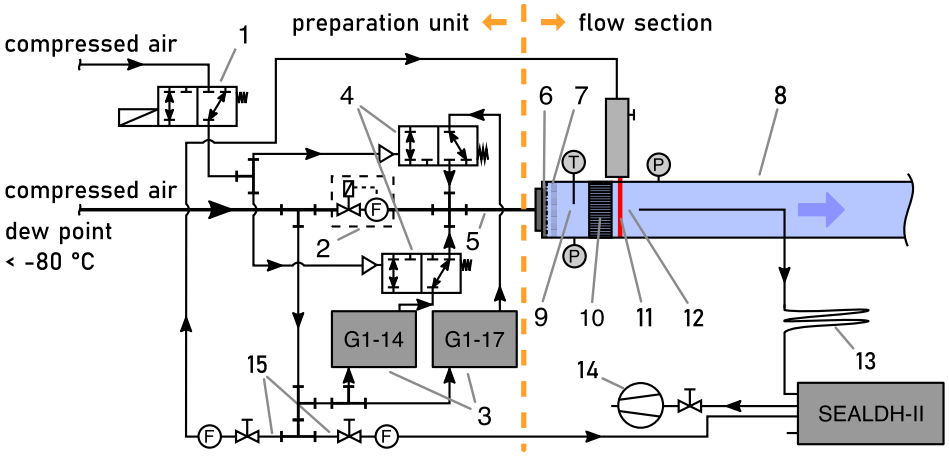


Figure 1: Pneumatic plan of the dynH_2O setup with the preparation unit on the left and the flow section on the right. 1. Solenoid valve, 2. Mass Flow Controller (MFC) for the carrier flow, 3. two two-pressure humidity generators, 4. two pneumatic valves, 5. position of the static mixing element, 6. Injector plate, 7. glass sintered filter, 8. dynamic test flow section, 9. temperature and pressure sensors, 10. aluminium honeycomb element, 11. optical measurement plane of the in situ MANTA-LAH instrument, 12. Gas inlet of the probe of SELADH-II (extractive) and position of the device under test, 13. flexible stainless-steel tube, 14. vacuum pump for sample extraction with SEALDH-II, 15. tubes with dry compressed air to purge the optics of SEALDH-II and MANTA-LAH.

https://doi.org/10.5194/egusphere-2026-6133
Preprint. Discussion started: 20 November 2026
© Author(s) 2026. CC BY 4.0 License.

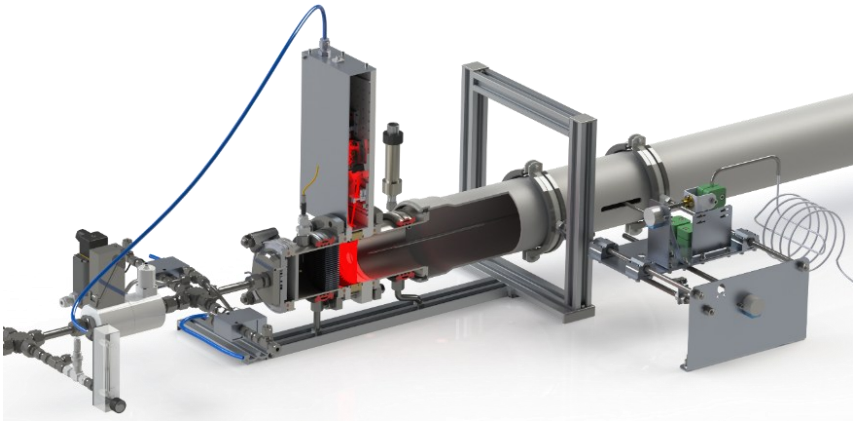


Figure 2: CAD rendering of the dynH_2O setup with cut through the flow section. Graphic modified from (Witt and Ebert, 2023).

2.1 Gas Humidity Preparation Unit

A dynamic calibration needs to be performed in a well-controlled gas flow system, that allows rapid, accurate and repeatable changes of the water vapor amount fraction. The preparation section of dynH_2O achieves this, by combining two two-pressure humidity generators (Model G1 from MBW, CH), each operated at a fixed, humidity level. Two fast pneumatic valves allow the flow to be switched between these generators and hence to step change between the two humidity levels defined by each of the G1 generators. The gas flow from the selected humidity generator is further mixed with a carrier and dilution gas flow of extra dry air (dew point < - 80 °C or < 0.5 ppm). The flow of the carrier gas is controlled with a calibrated mass flow controller (MFC). An electric solenoid valve is used to activate the two pneumatic valves. This way we avoid heating of the probe gas and enable a purely electric activation of the "gas switching" using a Lab-PC. Downstream of the pneumatic valves a static mixing element ensures that the gas flow from the humidity generator and the carrier gas flow are homogenized before the gas mixture enters the gas flow section with the DUT.

2.2 Gas Flow Section

The gas flow section of the dynH_2O setup consists of a stainless-steel injector plate, a glass-sintered filter, and an aluminium honeycomb structure. This device combination conditions the gas flow and ensures a spatially homogeneous velocity and concentration profile at the measurement plane (No. 6, 7 and 10 in Figure 1). The stainless-steel flow tube has an inner diameter of 80 mm and is 257 mm long. A 2000 mm long plastic pipe with an inner diameter of 103 mm is attached to the end of the stainless-steel flow section to prevent disturbances in the surrounding air from affecting the measurement zone (see Figure 2). The spatial homogeneity of the humidity and temperature in the flow section and the effects of remaining inhomogeneities have been investigated in detail, both experimentally and by using modelling approaches (Witt et al., 2023a). The LCrHS (DUT) are mounted directly behind the optical measurement plane of the MANTA-LAH dTDLAS hygrometer. The DUTs are placed upstream of and spatially close to the inlet of the extractive gas probe. This probe feeds into the SEALDH-II extractive dTDLAS hygrometer (Buchholz et al., 2016). Careful minimisation of the spatial separation between MANTA-LAH, DUTs and SEALDH-II minimizes temporal delays and the effects of the remaining spatial inhomogeneities.

2.3 Reference Measurements of H_2O, Pressure, and Gas Temperature

The primary H_2O reference instrument within dynH_2O is the sampling-free dTDLAS hygrometer MANTA-LAH. It is based on a circular multi-pass laser absorption cell (CMPAC) described in (Tuzson et al., 2013; Manninen et al., 2012). However,

https://doi.org/10.5194/egusphere-2026-6133
Preprint. Discussion started: 20 November 2026
© Author(s) 2026. CC BY 4.0 License.

instead of sucking the gas into an encapsulated CMPAC, we developed an open-path "oCMPAC" to avoid any gas sampling. Our oCMPAC is inserted into the gas flow, with the optical measurement plane oriented perpendicular to the flow direction. Combined with our dTDLAS evaluation (Buchholz et al., 2017) we determine SI-traceable, calibration-free, in-situ H_2O amount fraction measurements with up to 100 Hz temporal resolution. For our oCMPAC cell we used the reflective ring of a commercial CMPAC (IRsweep, CH). This ring cell has a free inner diameter of 80 mm and uses 51 reflections, resulting in a total optical path length of 3.986 m. This ring we then upgraded with our own aperture mask, coupling optics and a special mechanical integration into the gas flow section. Gas pressure is measured by two high-sensitivity, high-speed pressure sensors, one located upstream and one downstream of MANTA-LAH's optical measurement plane. Gas temperature we simultaneously measure with two techniques: A slow, high-accuracy PT100 platinum resistance thermometer, providing absolute gas temperature under static conditions. Fast T-changes during humidity steps we measure with fast, small diameter (0.5 mm) thermocouples. Both T-sensors are positioned directly upstream of the MANTA-LAH optical measurement plane. The signals from the photo detector, temperature and pressure sensors are digitized and stored and evaluated by the lab PC. The dTDLAS evaluation method is described in the section 3.2. In our measurements MANTA-LAH covers an H_2O amount fraction range from 100 ppm to 11000 ppm. The H_2O uncertainty is ±4.5 % (k = 2) and dominated by the time-invariant H_2O line strength uncertainty (Buchholz et al., 2016).

Due to our good spatial homogeneity of the gas flow, we can interpret the MANTA-LAH - H_2O amount fraction as the spatial average over the full cross section of the gas flow. For applications with less homogenous spatial H_2O distribution or gas temperature, we described a more refined approach in (Witt et al., 2023a).

2.4 Extractive H_2O Reference dTDLAS Spectrometer: *SEALDH-II*

As a second SI-traceable reference instrument, particularly suited for static calibration conditions, the extractive hygrometer SEALDH-II (Buchholz et al., 2016; Buchholz et al., 2014) is integrated into dynH_2O. SEALDH-II is an autonomous, first-principles dTDLAS hygrometer that covers a humidity measurement range from 3 to 40,000 ppm with a calculated maximum measurement uncertainty of ±4.3 % (k=2). A flexible stainless-steel tube (length: 700 mm, inner diameter: 2.4 mm) connects SEALDH-II with the inlet of the gas sampling probe, positioned downstream of the optical plane of the MANTA-LAH instrument. A vacuum pump reduces and stabilizes the pressure inside SEALDH-II's gas cell to 100 mbar. This ensures critical flow conditions at the orifice of the probe inlet, which leads to a constant sample gas flow of 0.5 standard litres per minute (SLM). Under these conditions, the calculated time to flush the SEALDH-II gas cell once is 3.6 s. The transfer optics of MANTA-LAH and SEALDH-II are continuously purged with dry compressed air (H_2O < 0.5 ppm) to minimize "parasitic" optical effects which cause instable H_2O offsets (Buchholz and Ebert, 2014). SEALDH-II is particularly valuable for the static calibration points of the MetDyHuCal procedure, because it has been extensively validated against the German national primary water vapor standard (Buchholz et al., 2014). Further it covers a wider H_2O range than MANTA-LAH, which extends our static calibration range.

2.5 Complete Dataset of a Calibration Run

The combination of instruments and sensors described above, yields a large, comprehensive dataset for each calibration run, which includes: a) fast, in-situ H_2O amount fractions measured upstream of the DUT by MANTA-LAH b) local, extractive H_2O amount fractions measured downstream of the DUT by SEALDH-II c) slow, accurate gas temperatures from the PT100 d) fast, relative gas temperature from the thermocouples; e) two gas pressures, upstream and downstream of the optical measurement plane f) gas flow rates from the two humidity generators and the carrier gas MFC, g) DUT measurements; h) 2D flow simulation data, which are used to estimate the ideal step response of the DUT in the absence of signal attenuation effects. i) Further we store all averaged raw H_2O absorption profiles at a time resolution of 30 Hz for MANTA-LAH and 10 Hz for SEALDH-II. Hence, any improvement in the dTDLAS evaluation process or in the molecular H_2O line strength or pressure

https://doi.org/10.5194/egusphere-2026-6133
Preprint. Discussion started: 20 November 2026
© Author(s) 2026. CC BY 4.0 License.

broadening data can be exploited for an improved re-evaluation of our two reference spectrometers, without the need for new measurements. The number of raw profiles averaged prior to saving and during the data evaluation can be adapted to match the DUT response time. Without any averaging, the raw scans can be saved at 139 Hz, the modulation frequency of the laser. Less averaging increases the required disc space, but enables a data re-valuation with higher variable temporal resolution.

3 Theory

3.1 Humidity Quantities and their Interconversion

The H_2O amount fraction c is defined as the ratio of the number of moles of water vapor to the total number of moles in a gas mixture and is expressed in the unit micromol per mol (µmol/mol), commonly referred to as parts per million (ppm). This quantity is independent of temperature and pressure, which makes it the preferred quantity for primary measurement standards and for direct spectroscopic measurements. Throughout this paper, the term ppm is used as a shorthand for µmol/mol.

All LCrHS investigated in this work report relative humidity, rH. To compare amount fractions (in ppm) measured with MANTA-LAH, rH is converted using the equations for the water vapour saturation pressure, H_2O_{sat} , provided by Sonntag and the enhancement factor, f, by Greenspan (Sonntag, 1990; Greenspan, 1976). f corrects for non-ideal gas behaviour, when water vapor is mixed with CO_2-free air and defines the ratio between H_2O_{sat} in air and H_2O_{sat} in pure water vapor. Multiplying the calculated saturation pressure, e, corrected with the enhancement factor f with the relative humidity yields the water vapor partial pressure e' which can then be divided by the ambient pressure p near the DUT to get the H_2O amount fraction value c (see Eq. 1).

$$c = \frac{e \cdot f}{p} = \frac{e\prime}{p} \quad (1)$$

The equations from Sonntag and Greenspan both introduce small additional uncertainties, which are propagated though the conversion steps. Additional uncertainty contributions originate from the pressure and temperature measurements. The metrological uncertainty calculations are performed in accordance with the Guide to the Expression of Uncertainty in Measurement, GUM (BIPM, 2008).

3.2 Absolute Humidity Measurement by SI-traceable dTDLAS

Our humidity reference values for the MetDyHuCal procedure are measured by dTDLAS-hygrometers that are traceable to the SI. The fundamental dTDLAS operating principle and the specific instrument realization used here have been described in (Witt et al., 2021b; Buchholz et al., 2017; Ebert, 2006; Ebert and Wolfrum, 2001) aspects most relevant for this paper are summarized below.

dTDLAS is based on the spectrally resolved absorption of near-infrared laser light by water vapor molecules in a gas. This is realized by wavelength-selected fiber-coupled distributed feedback (DFB) diode lasers which provide very narrow emission linewidth enabling high chemical selectivity. The laser emission is rapidly scanned by a periodical modulation of the diode laser current and sweeps the laser wavenumber across a carefully selected H_2O absorption line. This laser beam is directed through the gas sample onto an InGaAs photodetector. The light intensity $I(\nu)$ impinging the photodetector at each wavenumber ν is described by an "extended" version of the Lambert-Beer law:

$$I(\nu) = E(t) + I_0(\nu) \cdot Tr(t) \cdot exp[-S(T) \cdot g(\nu - \nu_0) \cdot N \cdot L] \quad (2)$$

here $I_0(\nu)$ is the light intensity in the absence of absorption, $S(T)$ is the temperature-dependent spectral line strength of the targeted H_2O transition, $g(\nu - \nu_0)$ is the area-normalized line shape function, N is the number density of absorbing molecules, and L is the optical path length inside the gas sample. Two additional terms distinguish the extended Lambert-Beer law from its standard form: $E(t)$ accounts for stray light and background radiation reaching the photodetector, and $Tr(t)$ is a transmission factor that covers spectrally broadband absorptive losses e.g. arising from particle absorption, mirror or window

https://doi.org/10.5194/egusphere-2026-6133
Preprint. Discussion started: 20 November 2026
© Author(s) 2026. CC BY 4.0 License.

contamination. $E(t)$ we determine at the beginning of each laser scan, where we drive the laser current below the threshold, so that the laser output is zero and the isolated background signal can be recorded.

Combining Equation 2 with the amount fraction definition and the ideal gas law yields the H_2O amount fraction c:

$$c = -\frac{k_B \cdot T}{S(T) \cdot L \cdot p} \underbrace{\int ln\left(\frac{I(\nu)-E}{I_0(\nu) \cdot Tr}\right) \frac{d\nu}{dt} dt}_{A_{line}} \quad (3)$$

here k_B is the Boltzmann constant, T is the gas temperature, p is the total gas pressure, and ν is the time-variable, scanned wavenumber. The spectral integral over the normalized absorption signal corresponds to the integrated line area A_{line}. The dynamic tuning behaviour $d\nu/dt$ of the laser depends on laser current and tuning speed and needs to characterized experimentally. $d\nu/dt$ is needed to transfer the measured absorption profile from the linear time axis onto a linear wavenumber axis, where the spectral integration is well defined. $d\nu/dt$ is fairly constant even over long time spans and is determined using a wavenumber reference scale created by a so called "etalon". The remaining free parameters in (3), including the line area, the pressure dependence of the "Voigt" line shape, and the polynomial coefficients describing laser power and thus the absorption baseline $I_0(\nu)$, are determined by fitting a physical model to each measured absorption profile.

The H_2O absorption line at 7299.43 cm-1 (1369 nm) was selected for several reasons: It exhibits minimal spectral interference from other atmospheric species or neighbouring H_2O lines, it falls within the wavelength range of cost-effective, very high-quality and long-term stable telecommunications DFB lasers and InGaAs detectors operating near room temperature, and the spectroscopic line parameters are accurately known. The line strength S(T) and related spectral data are derived from our own measurements (Buchholz et al., 2014; Hunsmann et al., 2006; Nwaboh et al., 2021a; Pogány et al., 2015). If otherwise not available, we take it from the most recent version of the HITRAN spectral database (Gordon et al., 2026). Even though our main H_2O line is well isolated, the spill-over effects from neighbouring H_2O lines just outside of the covered laser range have to be considered to ensure high measurement accuracy. At total pressures which cause significant pressure broadening and prohibit the application of a pure doppler line shape the consideration of additional H_2O lines is especially important. Our spectral model considers a total of 20 H_2O lines within the laser scan, some partially outside but neighbouring to the scan edges (see (Witt et al., 2021b; Ebert and Wolfrum, 2001) for more details).

Because all quantities on the right-hand side of Equation 3, namely T, p, L, S(T), E, Tr and $d\nu/dt$, are either directly measured with instruments traceable to SI units or are taken from validated spectroscopic publications or databases, dTDLAS measurement do not need to be calibrated with water vapour standards and constitute a primary method. The H_2O amount fraction is obtained directly from first principles without recourse to calibration gas mixtures or humidity generators, establishing an unbroken traceability chain to the SI. dTDLAS spectrometers working with this principles are also termed OGS, "Optically defined gas standards" (Nwaboh et al., 2021b).

3.3 Model Equation for the Dynamic Sensor Response

In addition to a static calibration at fixed humidity set points, the MetDyHuCal procedure characterizes the dynamic response of each DUT by analysing its output during controlled, traceable gas humidity steps. When the humidity is changed from one level to another, the sensor output y(t) is expected to follow a first-order exponential approach of the form:

$$y(t) = b + k \cdot \left(1 - e^{-\frac{t}{\tau}}\right) \quad (4)$$

here b is the initial sensor output at the time of the step change, k is the total amplitude of the step response (corresponding to the difference between the new and old equilibrium values), and τ is the time constant that characterizes the dynamic sensor response. To extract τ we fit this model to our measured step response (after attenuation effects from the setup itself have been removed (see section 4.2)). τ quantifies delays introduced by processes such as water adsorption or desorption at the DUT sensing surface or housing.

https://doi.org/10.5194/egusphere-2026-6133
Preprint. Discussion started: 20 November 2026
© Author(s) 2026. CC BY 4.0 License.

4 Experiments

4.1 Tested LCrHS Sensors

A total of 48 individual LCrHS were statically and dynamically characterised as part of this study. The tested sensors represent 9 different models from 8 manufacturers, spanning a price range from 1.29 € to 30.80 € per unit. For each sensor model we tested between 4 and 8 individual sensors. Table 1 provides an overview of the sensor models, their manufacturers, and the key specifications reported by the manufacturer in the respective datasheets.

The dynH_2O setup allows to characterise four sensors simultaneously during each test run. Each sensor is read out via an individual Arduino Nano Every microcontroller. 8 from 9 tested sensor models use a digital communication protocol, either I^2C or, in the case of the DHT22, a 1-Wire protocol. The HIH4000 provides an analogue voltage output that was digitised using the on-board ADC (10 bit 150 ksps) of the Arduino microcontroller.

To minimise the effects of hidden on-sensor data processing, all on-sensor filtering and averaging functions, as well as filtering functions in the communication libraries, were disabled when possible. The raw sensor data were transferred to the laboratory PC via an USB serial connection without any additional smoothing. All sensors were read out at the highest data acquisition rate permitted by the respective communication protocol and consistent with the datasheet recommendations, resulting in sampling frequencies from 2 Hz to 50 Hz depending on the sensor model.

Active sensor heating, an optional function available on several of the tested models to avoid condensation, was disabled throughout all our experiments. Non-condensing conditions were ensured at all times via our experimental conditions. Heater deactivation also improved the comparability between sensor models and reflects the default operating-mode in the majority of field deployments. All tested sensors unfortunately suppress “negative” humidity values in the firmware. This made meaningful zero-point calibrations impossible, because negative fluctuations of the electronics output are supressed, which creates a positive bias of the averaged sensor output at zero.

https://doi.org/10.5194/egusphere-2026-6133
Preprint. Discussion started: 20 November 2026
© Author(s) 2026. CC BY 4.0 License.

Table 1: Sensor manufacturer and type overview, including manufacturer specifications for the tested sensors.

Information from the Datasheet of the Manufacturer *							additional information		
Sensor Model	Manufacturer	Range in % rH	Accuracy in % rH	τ_{63} in s **	Drift in % rH/yr	Meas. quant. ***	Price est.****	No. tested	Example use cases
AHT10	ASAIR	0 - 100	2	8 [1]	< 0.5 [2]	T	1.29 €	4	(Gupta et al., 2024) (Hartono and Utama, 2025)
BME280	Bosch	0 - 100	3	1 [1]	0.5	T, P	12.00 €	6	(Holovatyy, 2021) (Sari et al., 2023)
DHT22, AM2302	ASAIR	0 - 99.9	2	8 [3]	1	T	7.00 €	6	(Koestoer et al., 2019)
HDC1080	Texas Instruments	0 - 100	2	15 [4]	0.25 [5]	T	1.90 €	8	(Santos Jr et al., 2025) (Mihajlo et al., 2020)
HIH4000	Honeywell	0 - 100	3.5	5 [6]	no data	none	30.80 €	4	(Nikolaev et al., 2018) (Zhang et al., 2014)
HTE301	E+E	0 - 100	1.8	5 [1]	< 0.5	T	5.80 €	4	
HTE501	E+E	0 - 100	1.8	5 [1]	< 0.5	T	6.40 €	5	(E+E Elektronik GmbH, 2022)
HTU21D	TE connectivity	0 - 100	2	5 [7]	0.5	T	3.80 €	5	(Wiyagi et al., 2017) (Wang et al., 2015)
SHT31-D	Sensirion	0 - 100	2	8 [1]	< 0.25	T	3.20 €	6	(Macagga et al., 2024) (Hossain et al., 2025)

*: Used manufacturers datasheets (top to bottom): (ASAIR, 2018); (Bosch, 2024); (ASAIR); (Texas Instruments, 2016); (Honeywell International Inc., 2010); (E+E Elektronik GmbH, 2023a); (E+E Elektronik GmbH, 2023b); (TE Connectivity, 2017); (Sensirion, 2022)

**: τ: Time the sensor needs to reach 63 % of the final response after a H2O step change in the surrounding air, as reported in the datasheet by the manufacturer. For a sensor with perfect first order response this value is identical, regardless of the amplitude of the step change. This parameter is also known as a time constant.

***: additional sensor signals / measured besides relative humidity.

****: Individual price derived from online data. Prices vary widely depending on the vendor or the quantity ordered.

1: At 25 °C with 1 m/s air speed.

2: Only valid when operated between 0 and 80 % rH.

3: No information on type / conditions of response time.

4: No information on temperature or air speed.

5: Valid at 30 °C between 20 and 50 % rH.

6: Datasheet: “Measured in slow moving air”, but no air speed value is provided.

7: Determined from a step change from 33 to 75 % rH with an air speed of 1 m/s.

4.2 Test Procedure and Data Evaluation

The overarching goal of the new MetDyHuCal calibration procedure is to perform a traceable characterisation of the static and dynamic response of the LCrHS in a single setup and process. Each H_2O step is held until stable values needed for the static calibration are reached. The switching between the static amount fraction levels is performed much faster than the DUT response time and is used for the dynamic characterisation of the sensors. A fully automated test programme was developed to characterize the selected LCrHS. A complete LCrHS characterization run with up to four DUT takes approximately 4.5 hours, so that the effective characterization per sensor can be as low as 1.1 hours.

Our static calibration protocol comprises six H_2O levels between 100 ppm and 14000 ppm, with SEALDH-II serving as traceable H_2O reference. For some LCrHS we found large measurement offsets or output clipping at low H_2O values. In these cases we rose the lowest H_2O test levels to ensure the full sensor functionality.

https://doi.org/10.5194/egusphere-2026-6133
Preprint. Discussion started: 20 November 2026
© Author(s) 2026. CC BY 4.0 License.

Our dynamic characterization protocol is realized using the fast transitions between the static H_2O setpoints and uses MANTA-LAH as a traceable dynamic H_2O reference. Hence, static and dynamic characterizations are embedded in a single test sequence. Dynamic characterizations at different H_2O levels also reveal a possible amount fraction dependence of the dynamic response.

We developed a two-dimensional flow simulation of the water vapour amount fraction front propagating through the flow section, to further optimize the dynamic characterization and to make the dynamic characterisation results independent of the specific geometric distance between the MANTA-LAH optical plane and the DUT position in the flow channel, as described in (Witt et al., 2023b). The simulation takes the measured H_2O amount fraction front at the optical plane of MANTA-LAH as its input and computes the local amount fraction dynamics at the DUT location thereby removing any deviation caused by the characteristic response time contributions of the dynH_2O setup itself. This DUT-"localized" H_2O dynamics is then compared to the measured LCrHS response and used for a time-domain correction, by shifting the response curve to match the output that would be expected from a sensor subjected to an infinitely fast, ideal step change.

Relative humidity values reported by the LCrHS are converted to H_2O amount fractions as described in section 3.1. When a sensor also provides gas temperature and pressure, we use the sensor p,T-values in the rH to amount fraction conversion. Otherwise, the temperature and pressure data from the flow channel instrumentation are used.

4.3 Measurement Uncertainties

The uncertainties of all derived quantities are evaluated in accordance with the principles of the *Guide to the Expression of Uncertainty in Measurement* (BIPM, 2008). Standard uncertainties are assigned to all input quantities, and the combined standard uncertainty of each output quantity is obtained by propagating these through the respective measurement model.

Specifically, the uncertainties of the input parameters are combined with the uncertainty arising from the conversion of relative humidity to H_2O amount fractions (see Section 3.1), as well as the contributions from the static calibration fit and the fitting of the model equation describing the dynamic sensor behavior (Eq. 4). We perform these fits using a least-squares approach implemented in Python that explicitly accounts for the measurement uncertainties of all input quantities. This method follows the general formulation of Nielsen (Nielsen, 2002), in which the estimates and their associated standard uncertainties - represented in a covariance matrix - constitute the input to the minimization problem.

The resulting calibration functions and dynamic model parameters thus carry fully propagated, traceable uncertainties. All uncertainties reported in this work are *expanded uncertainties*, calculated with a coverage factor of ($k = 2$) to provide a coverage interval of approximately 95 %. Uncertainties are determined for each individual sensor; where median results for a specific sensor model are reported, the associated uncertainties represent the median of the individual sensor uncertainties.

5 Results

5.1 Static LCrHS Calibration

Figure 3 shows the static calibration data for all individual sensors of the models HTE501 (left, 5 sensors) and SHT31-D (right, 6 sensors). This comparison demonstrates the diversity in sensor linearity and accuracy found across the sensor models tested in this paper. The LCrHS rH values, converted to H_2O amount fraction, are plotted against the traceable reference values simultaneously determined with SEALDH-II. Our computed measurement uncertainties are shown on the y and x-axis.

Each sensor data set was fitted with a second-order polynomial using the uncertainty-weighted least-squares method described in section 4.3. The narrow, dark-shaded region in each plot (see insets) represents the range covered by the individual 2^{nd}-order polynomial fits of all sensors of the same model. The light-shaded regions indicate the range of the 95 % coverage intervals for the sensors of the ensemble. The residuals between individual measured data points and the individual sensor polynomial fits are shown below each regression plot.

https://doi.org/10.5194/egusphere-2026-6133
Preprint. Discussion started: 20 November 2026
© Author(s) 2026. CC BY 4.0 License.

These two sensor types nicely show the contrasting behaviour in terms of linearity and accuracy among the tested sensor models. The SHT31-D sensors (Figure 3, right) show a pronounced non-linear response. To ensure a consistent evaluation, a 2nd-order polynomial correction was applied to all sensors in the subsequent dynamic evaluation, regardless of whether some individual specimen were suitable for a first-order correction. The static calibration results for all sensor models are summarized in Table 2. To keep the presentation concise, Table 2 reports only the coefficients of the 1st-order polynomial fits.

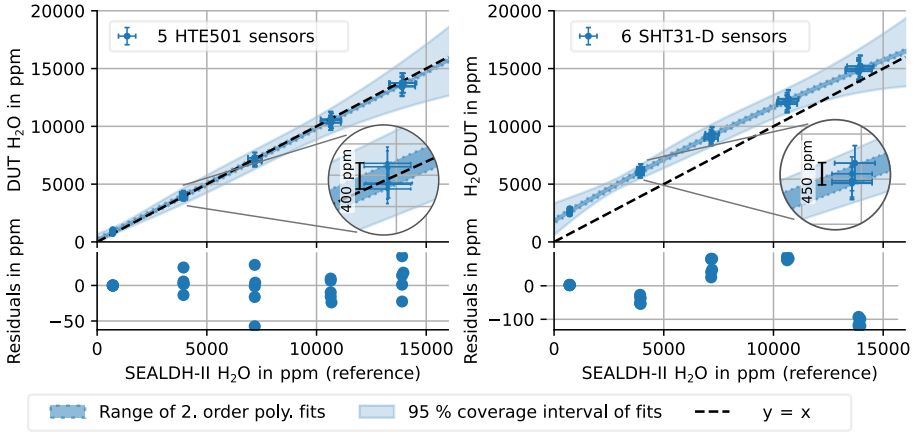


Figure 3: Regression plots showing static H_2O amount fractions of five HTE501 sensors (left) and six SHT31-D sensors (right) referenced to SEALDH-II. Each sensor data set was fitted with a 2nd-order polynomial, taking into account x- and y-axis uncertainties at each data point. The range of the individual sensor polynomials is shown as dark-shaded area surrounded by the range of the 95 % coverage intervals shown in dark blue (see also insets). Absolute residuals (in ppm) between measured data and the 2nd-order polynomial fit are shown below. While HTE501 is very linear, SHT31-D shows a pronounced 3rd order dependence, which is not fully covered by our fit and shows up in the residuals shown below.

https://doi.org/10.5194/egusphere-2026-6133
Preprint. Discussion started: 20 November 2026
© Author(s) 2026. CC BY 4.0 License.

Table 2: Static characterisation data for all sensor models. Each individual sensor is fitted with a 1st-order polynomial. The fit parameters variation within the model ensemble (= between all specimen of a model) is characterized via the median value, the largest and smallest value and the absolute uncertainty of the median for the slope and the offset derived from the fit. $-log(1-R^2)$ quantifies the linearity averaged over the model ensemble. The higher $-log(1-R^2)$, the better the linearity of the sensor model. The best results in a column are highlighted in bold, the worst are underlined. Note: The high offset values of almost ±2000 ppm compared to the covered range of a few 100 to 15000 ppm.

		Slope [ppmREF/ppmDUT]			Offset [ppm]				
Sensor Model	No. of tested sensors	median value	max min	median uncert. (k=2)	median value	max min	median uncert. (k=2)	-log (1-R^2)	rel. median uncert. *
AHT10	6	0.856	0.991 0.813	0.062	1612.4	1705.3 220.6	163.6	6.92	14.9 %
BME280	6	1.084	1.103 1.072	0.050	-799.0	-194.1 -887.4	67.1	7.49	11.4 %
DHT22, AM2302	5	0.814	0.828 0.804	0.061	892.4	1104.2 516.4	197.0	5.73	17.8 %
HDC1080	10	0.788	0.815 0.746	0.035	**-271.0**	-8.6 -772.3	**43.3**	5.82	**8.5 %**
HIH4000	4	1.068	**1.075** **1.062**	0.053	-1287.3	-1027.7 -1436.9	91.6	8.38	11.1 %
HTE301	4	1.099	1.120 1.093	0.052	-830.4	-351.7 -991.2	69.1	**10.67**	11.0 %
HTE501	5	**1.040**	1.057 1.034	0.046	**-199.5**	-33.2 -371.0	**41.0**	**10.87**	**10.2 %**
HTU21D	4	0.969	0.990 0.958	0.071	1443.2	**1608.2** **1287.2**	173.2	7.49	16.5 %
SHT31-D	6	**1.026**	**1.035** **1.024**	0.055	-1935.1	-1762.0 -2292.6	125.5	7.60	11.9 %

*: Relative median value of the uncertainty of the measured and converted H_2O amount fraction between 1000 and 14000 ppm (calculated as average over the concentration span and as median over all individual sensors of the same model).

5.2 Dynamic LCrHS Characterisation

Typical raw amount fractions (here HDC1080_01a) and both dTDLAS reference instruments SEALDH-II and MANTA-LAH during one run of the automatic dynamic characterisation are depicted in Figure 4. The left panel shows the time dependent H_2O amount fraction over the full concentration range. The right panel shows a close-up of the first concentration step. Here, the LCrHS time axis has been corrected using the flow simulation as described in section 4.2. The small size of HDC1080 allows the sensor to be placed closer to the optical plane of MANTA-LAH, leading to a peak LCrHS time correction of only 0.27 s, which is not resolvable in Figure 4. Nevertheless, it is highly relevant for the determination of the characteristic time τ.

https://doi.org/10.5194/egusphere-2026-6133
Preprint. Discussion started: 20 November 2026
© Author(s) 2026. CC BY 4.0 License.

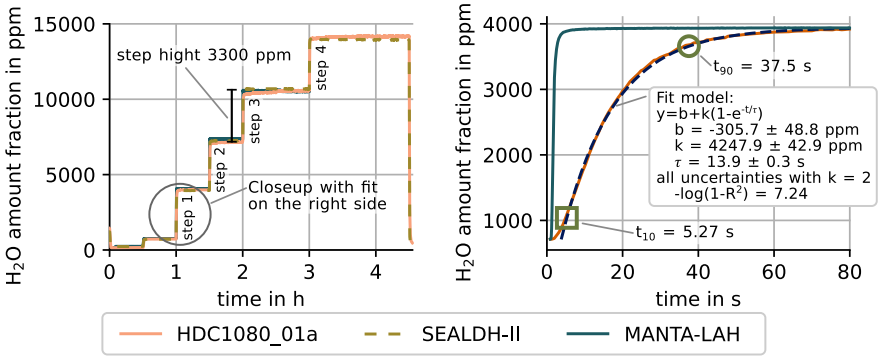


Figure 4: Left: H_2O vs time for MANTA-LAH, SEALDH-II and one LCrHS (HDC1080_01a) over a complete run of the measurement program. Right: Close-up of the response to the first step shown on the left with a fitted 1st order model (Eq. 4).

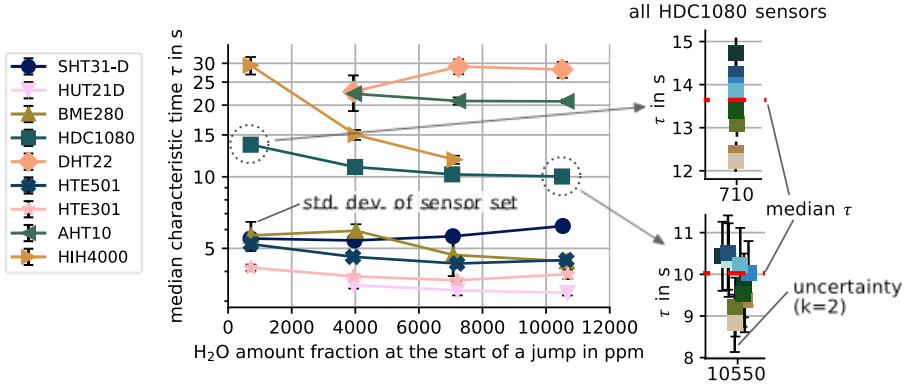


Figure 5: MetDyHuCal results: Median characteristic sensor response time τ for each LCrHS model determined at the different H_2O amount fraction steps. The error bars indicate the standard deviation between the responses of each individual sensor of the same model. The X-axis shows the average H_2O amount fraction at the beginning of the steps. Each step has a step hight of 3000 ppm. The plots on the right show the fitted τ values for each individual sensor of model HDC1080, the median value, and the expanded measurement uncertainty (k = 2) of τ at the lowest (710 ppm) and the highest (10550 ppm) H_2O amount fraction.

τ is determined by fitting the 1st-order model (Eq. 4) to the LCrHS data in the range of 10 % to 99 % of the final step hight. The fitted model is plotted as dashed blue line in Figure 4 (right). From this fit we derive a characteristic time τ = 13.9 s ± 0.3 s (k=2). We quantify the "goodness" of the fit via $-log(1-R^2)$, where R^2 is the fit's coefficient of determination. The plot highlights the very steep H_2O changes realized with our dynH_2O setup, and the high time resolution of MANTA-LAH, thanks to the sampling-free, open-path measurement: The steepest temporal H_2O gradient measured by MANTA-LAH in dynH_2O in Figure 4 amounts to 3950 ppm/s.

The data processing - as illustrated in the right panel of Figure 4 - is repeated for all concentration steps of all 48 tested LCrHS. The resulting τ values are clustered by sensor model and the median τ values of each sensor model are plotted vs the H_2O amount fraction at the beginning of each concentration step (see Figure 5, H_2O amount fraction dependence of the dynamic behaviour). The error bars in Figure 5 represent the standard deviation of τ among the individual sensors of the same model. The inset to the right shows individual τ values at the lowest and the highest H_2O level for all HDC1080 sensors, together with the median τ and the expanded uncertainties (k = 2) for each τ. The H_2O-dependence of τ (see Figure 5) varies over the different sensor models. The τ -value-spread between low and high humidity varies from 6 to 60 % depending on sensor type.

https://doi.org/10.5194/egusphere-2026-6133
Preprint. Discussion started: 20 November 2026
© Author(s) 2026. CC BY 4.0 License.

The results of the full dynamic characterisation of all 8 sensor types are summarised in Table 3. For each sensor model, the median of τ and the median of the relative expanded uncertainty (k = 2) are reported, for the lowest H_2O amount fraction (710 ppm), the highest (10550 ppm), as well as across all measured steps. The maximum and minimum τ values among the individual sensors of the same model are also given, together with the relative spread in τ defined as $(\tau_{max} - \tau_{min})/\tau_{median}$. The rightmost column shows the relative deviation of the overall median τ from the time constant reported in the manufacturer datasheet.

Table 3: Results of our dynamic characterisation by sensor model. The median values of the characteristic time τ are shown determined from the step response starting at 710 ppm and 10550 ppm as well as overall measured step responses. For each τ value the average relative measurement uncertainty with k = 2 is shown as well as the maximum and minimum determined τ value (or the results from the fastest and slowest individual sensor from that model). The column on the right shows the relative difference between the "overall τ" and the τ value that was provided in the data sheet of the manufacturer. A positive value here indicates that the determined response time was slower than the time provided by the manufacturer and vice versa. The best results (fast response times, small spread or small difference to the values from the manufacturer) in each column are highlighted with bold lettering, and the worst results are underlined.

manufacturer information		measured at 710 ppm			measured at 10550 ppm			over all steps			rel. diff. to manufac. τ
model name	τ [s]	median τ [s] rel. u.	τ_{max} τ_{min} [s]	$\frac{\tau_{max}-\tau_{min}}{\tau_{median}}$	median τ [s] rel. u.	τ_{max} τ_{min} [s]	$\frac{\tau_{max}-\tau_{min}}{\tau_{median}}$	median τ [s] rel. u.	τ_{max} τ_{min} [s]	$\frac{\tau_{max}-\tau_{min}}{\tau_{median}}$	
AHT10 [1]	8	22.34 ± 7.1 %	23.38 21.15	10.0 %	20.76 ± 13.8 %	21.22 20.11	5.4 %	20.83 ± 10.0 %	23.75 20.11	**17.5 %**	61.6 %
BME280	1	5.67 ± 4.4 %	7.67 5.26	42.4 %	4.41 ± 23.7 %	4.71 4.18	12.0 %	5.18 ± 11.3 %	7.67 3.50	80.5 %	80.7 %
DHT22, AM23021	8	22.79 ± 7.3 %	29.82 19.08	47.1 %	28.24 ± 13.1 %	29.41 22.93	22.9 %	28.24 ± 10.3 %	31.26 19.08	43.1 %	71.7 %
HDC1080	15	13.64 ± 2.2 %	14.75 12.24	18.4 %	10.03 ± 8.0 %	10.52 8.82	16.9 %	10.62 ± 5.3 %	14.75 8.82	55.8 %	-41.3 %
HIH4000 [2]	5	29.39 ± 4.4 %	32.89 26.83	20.6 %	11.80 ± 7.1 %	12.71 11.46	10.6 %	15.02 ± 6.7 %	32.89 11.46	142.7%	66.7 %
HTE301	5	**4.15** ± 3.9 %	4.35 4.05	**7.3 %**	**3.90** ± 19.3 %	3.68 3.60	**1.9 %**	**3.86** ± 10.1 %	4.35 3.60	19.4 %	**-29.7 %**
HTE501	5	5.21 ± 3.4 %	5.70 5.20	9.5 %	4.47 ± 16.2 %	4.62 4.41	**4.7 %**	4.54 ± 8.5 %	5.70 3.87	40.3 %	**-10.2 %**
HTU21D [1]	5	**3.51** ± 12.0 %	3.66 3.38	8.0 %	**3.25** ± 36.5 %	3.32 3.07	7.5 %	**3.33** ± 21.3 %	3.66 2.98	20.3 %	-50.1 %
SHT31-D	8	5.50 ± 4.2 %	5.54 5.34	**3.6 %**	6.21 ± 13.4 %	6.30 6.00	4.8 %	5.56 ± 8.6 %	6.30 5.34	**17.1 %**	-43.8 %

1: The sensor was not able to deliver data at 710 ppm. The first step for these sensors is therefore the next step that started at 3900 ppm.

2: The sensors did not deliver reliable data during the measurements with the highest H_2O amount fraction. The results for the high water vapour content is therefore reported for the step starting from 7100 ppm.

https://doi.org/10.5194/egusphere-2026-6133
Preprint. Discussion started: 20 November 2026
© Author(s) 2026. CC BY 4.0 License.

6. Discussion

6.1 Static Calibration Results

Our static calibrations reveal substantial measurement offsets and non-ideal higher order slopes across all tested sensor models, which underlines the necessity for an individual sensor calibration prior to deployment. Among the most striking examples are the SHT31-D and HTU21D sensors, for which offsets of more than 1000 ppm were found for every individual sensor. This finding illustrates that systematic deviations of low-cost sensors from the true humidity value can be large even for comparatively accurate and well-characterised sensor models.

The sensor models HTE301 and HTE501 exhibit the best H_2O linearity, with R^2 values of 0.999977 and 0.999981 respectively. Because all R^2 values in Table 2 are close to one we report $-log(1-R^2)$ values for easy linearity comparisons. The $-log(1-R^2)$ values of the HTE301 and HTE501 are 10.67 and 10.87 respectively. This clearly indicates that a first-order polynomial provides an excellent description of their response over the tested range.

By contrast, DHT22 and HDC1080 exhibit the lowest $-log(1-R^2)$ values, indicating a pronounced non-linear response so that a 2nd order (or even 3rd order) polynomial fit is recommended.

Although Table 2 shows only 1st-order fit parameters for comparability, the 2nd-order correction derived from the static calibration was applied to all sensors before the dynamic characterisation in order to minimise any residual static error.

The spread between the maximum and minimum offset found between individual sensors of the same model illustrates the limitations of using a single "representative" calibration data set for an entire sensor model. For the AHT10, this spread exceeds four times the median expanded uncertainty (k = 2) of the offset, showing that inter-unit variability is the limiting factor for the achievable uncertainty of this sensor model, rather than the calibration setup itself. The single, model-level corrections used by the manufacturer leave a significant systematic residual error between individual units that substantially exceed the expanded uncertainty of our calibration.

Together, our results point to a practical ranking of the tested sensor models. For accuracy-critical applications, the HDC1080 offers the best relative residual uncertainty of all models tested (8.5 %, k = 2) but it requires a second-order fit model. For accuracy-critical applications DHT22 seems least suited, combining the highest relative residual uncertainty (17.8 %) with a large offset (median 892 ppm) and pronounced non-linearity. HTE501 stands out for combining high linearity with small, consistent offsets (median -199 ppm), so that a 1st-order correction suffices. These advantages come at the cost of a higher unit price (6.40 €) compared to AHT10, HDC1080, or SHT31-D (1.29 – 3.20 €).

For deployment at scale, where individual calibration of every unit often is not practical, the AHT10 and HDC1080 are least suited, since a shared, model-level characterization converts their large inter-unit spread into substantial residual errors. Models with tighter inter-unit spread, (e.g. HUT21D or HTE501), therefore seem better suited for a large-scale deployment.

6.2 Dynamic Characterisation Results

Our results reveal that several sensor models show a pronounced τ-dependence on H_2O amount fraction.

HDC1080, for example, shows τ decreasing from a median of 13.64 s at 710 ppm to 10.03 s near 10550 ppm, a relative change in τ of about 26 %. HIH4000 is worse with τ decreasing from 29 s at low H_2O to 12 s at high H_2O (Figure 5), corresponding to a relative spread of 142.7 % to the median τ across the full range. This strong concentration dependence highlights the importance of performing dynamic characterisations at multiple concentration levels in order to generate dynamic calibration data that is representative over the full H_2O operating range.

Comparing the overall τ measured in dynH_2O with the manufacturer datasheet reveals considerable relative deviations, ranging from −50.1 % for HTU21D to +80.7 % for BME280 (Table 3). These discrepancies can often be attributed to housing design. Three of the four models for which the measured τ, exceed the datasheet value: AHT10, BME280, and DHT22 have a housing that partially covers the sensing element. AHT10 and BME280, restrict the gas exchange with the surrounding atmosphere to

https://doi.org/10.5194/egusphere-2026-6133
Preprint. Discussion started: 20 November 2026
© Author(s) 2026. CC BY 4.0 License.

a single pin hole, making the effective response time highly dependent on flow velocity and direction. The manufacturer-specified value was likely obtained under optimized flow conditions, favourable to fast gas exchange for the specific tested sensor model. Conversely, some sensors we found to be faster than specified, which is likely caused by the manufacturer characterisation with a much slower temporal H_2O gradient than dynH_2O offers. The fast H_2O step changes in our dynH_2O setup (3950 ppm/s) combined with our time-axis correction (described in Section 4.2), approximate an ideal, instantaneous H_2O-step.

The different systematic differences and the large inter-sensor variability clearly underline the need for a standardised test procedure for dynamic hygrometer characterisation.

Our results translate directly into selection guidance for time-critical applications:

HTU21D and HTE301 are the fastest sensor models tested, with a median τ of 3.33 s and 3.86 s, respectively. This makes these sensor models preferred candidates for applications requiring rapid tracking of humidity changes, such as in process control loops or for weather-balloon payloads with significand ascent and decent speeds.

DHT22 and AHT10 are the slowest (median τ of 28.24 s and 20.83 s) and are better reserved for slowly varying environments such as indoor climate logging or long-interval building monitoring.

The stability of τ across the dynamic H_2O measurement range from 710 ppm to 10550 ppm is a second, largely independent criterion. Here, SHT31-D shows the smallest relative τ-spread of all tested models (17.1 %). A single, concentration-independent time constant is a reasonable approximation for this sensor. The HIH4000 and BME280, by contrast, show the largest concentration dependence (142.7 % and 80.5 % spread, respectively) and must not be characterised or corrected with a single τ value if used across a wide humidity range. For these two models, multi-point dynamic calibration of the type demonstrated in this work is not an optional refinement but a precondition for a physically meaningful correction.

The reliability of the manufacturer-specified τ itself varies strongly between models. The HTE501 datasheet value is the most accurate, deviating from our measured τ by only −10.2 %, and can reasonably be used as a field estimate in the absence of a full dynamic calibration. The BME280 sits at the other extreme, with the largest datasheet deviation of any tested model (+80.7 %). Combined with its pinhole housing design and pronounced concentration-dependent τ, this indicates that the BME280's datasheet response time should not be relied upon for dynamic applications covering a wide H_2O range. Given how widely this sensor is used in applications such as radiosonde payloads (notably for its combined temperature/pressure output), individual dynamic sensor characterisation is highly advisable for such demanding use cases.

6.3 Uncertainty of the Results

The right column of Table 2 shows the relative median uncertainty (k = 2) of the H_2O amount fraction, derived for each sensor model in the H_2O range from 1000 to 14000 ppm. The uncertainty is calculated first as the average over the concentration span for each sensor and then combined by taking the median over all individual sensors of the same model. The expanded uncertainties (k = 2) range from 8.5 % for HDC1080 to 17.8 % for DHT22 and 16.5 % for HTU21D. The uncertainty differences between sensor models arise primarily from differences in short-term stability and noise and from the degree to which the sensor response can be described by a 1^{st}- or 2^{nd}-order polynomial.

The contributing uncertainty components that are common to all sensors include the (time invariant) measurement uncertainty of the SEALDH-II reference instrument (4.3 %, k = 2), the uncertainty introduced by Sonntag's vapour pressure formulation and Greenspan's enhancement factor used in the conversion, and the uncertainty of the gas temperature and pressure measurements used for the conversion from relative humidity to H_2O amount fraction (conservatively assumed to be 1 K and 1 hPa respectively) (Buchholz et al., 2016; Sonntag, 1990; Greenspan, 1976).

For the dynamic characterization the uncertainty of the time axis correction is included with ±0.1 s. The relative median expanded uncertainty for the τ values over all concentration steps (Tabel 3) range from 5.3 % for HDC1080 to 21.3 % for

https://doi.org/10.5194/egusphere-2026-6133
Preprint. Discussion started: 20 November 2026
© Author(s) 2026. CC BY 4.0 License.

HUT21D sensors. The largest contributing factor to the τ uncertainty is the shape of the step response and the applicability of a 1st-order dynamic model (Eq. 4).

6.4 Traceability and Performance of the dynH_2O Setup

dynH_2O provides traceability for the H_2O amount fraction through the MANTA-LAH instrument and for gas temperature, and gas pressure by the calibrated reference sensors in the flow channel. The time measurement performed by the laboratory PC is not yet formally traceable to a national standard; however, the expected uncertainty contribution from the PC timing to the time axis is expected to be two orders of magnitude smaller than the total uncertainty of the time axis (±0.1 s), making this contribution not significant for the characterisation of sensors with response times in the range of seconds. In its current configuration, the dynH_2O setup covers an H_2O amount fraction range from 100 to 14000 ppm for static calibrations and 100 to 11000 ppm for dynamic characterisation. The H_2O signal-to-noise-ratio (SNR) ranges from 150 at low H_2O amount fractions (100 ppm) to 600 at high amount fractions (11000 ppm) at the high temporal resolution of 30 Hz. The H_2O resolution of MANTA-LAH is 1.1 ppm, determined with a 1σ-SNR of 260 at 280 ppm (Witt et al., 2023b). During the generated H_2O steps, the maximum H_2O amount fraction change rate is 3950 ppm/s.

The reproducibility of our τ measurements was separately assessed via five repeated τ determinations per H_2O step, performed on 10 individual sensors across 15 different days and after repeated removal and reinstallation of the DUT into the setup. The median relative standard deviation of the determined τ values for each individual sensor is 1.0 % (mean: 1.3 %).

This reproducibility is significantly smaller than the measurement uncertainty of the individual τ values, which demonstrates that our MetDyHuCal procedure in combination with our dynH_2O setup is capable of resolving genuine differences between sensors rather than being limited by the setup/procedure repeatability.

These performance characteristics make the setup suitable for metrological characterisations under both static and dynamic conditions and for a broad range of humidity sensors.

7. Conclusion

This work presented MetDyHuCal, our new, integrated, metrological calibration procedure for a combined static and dynamic characterisation within a single procedure and in a single experimental setup, dynH_2O. The procedure was applied to the characterization of low-cost relative humidity sensors. We calibrated a total of 48 individual sensors from 9 different models and 8 manufacturers. All H_2O measurements were performed with MANTA-LAH, a sampling-free, open-path dTDLAS-hygrometer as the primary reference. The first-principle evaluation of this dTDLAS instrument, provides a direct link to fundamental physical quantities.

The total pure measurement time for the complete characterisation of all 48 sensors was approximately 56 hours. The data set comprised two dTDLAS spectrometers (MANTA-LAH and SEALDH II), four pressure sensors, four gas temperature sensors, plus up to four LCrHS sensors, which were simultaneously characterised in a single run. The two reference spectrometers stored raw spectra with time resolution of 33 ms (30 Hz) in the case of MANTA-LAH and 100 ms (10 Hz) in case of SEALDH-II. Over the course of our 56 h campaign, more than two million raw absorption spectra were fitted with a 20-absorption line spectral model and evaluated. More than 200 individual H_2O steps were isolated, simulated, fitted, and characterised.

All four objectives that were set out at the beginning of this work were achieved. 1st, a single unified setup was demonstrated to be capable of performing both static and dynamic calibrations in immediate succession, without any modification to the experimental configuration. 2nd, a dedicated procedure for the metrological dynamic characterisation of humidity sensors (MetDyHuCal) was developed, established, and validated. The method combines a highly controlled and repeatable, rapid H_2O amount fraction step generation, a two-dimensional flow simulation for correcting the sensor position relative to the dTDLAS optical plane, and an uncertainty-weighted first-order low-pass model fit to extract τ. 3rd, the fusion of the setup and

https://doi.org/10.5194/egusphere-2026-6133
Preprint. Discussion started: 20 November 2026
© Author(s) 2026. CC BY 4.0 License.

the method were demonstrated and applied to characterize a large, diverse set of LCrHS. We produced results that are directly comparable between sensor models and can challenge manufacturer data. 4th, a first comprehensive and traceable dataset for the comparison of the static and dynamic performance of LCrHS was generated.

Our dynH_2O setup covers an H_2O amount fraction range from 100 to 14000 ppm for static calibrations and 100 to 11000 ppm for dynamic characterisations. The fastest H_2O amount fraction change rate was 3950 ppm/s. The reproducibility of the dynamic characterisation was determined by repeated characterisation of 10 sensors, each measured five times on different days. Between subsequent calibration all sensors were removed and reinstalled in the setup, to include handling and installation uncertainty. The reproducibility test for the characteristic time constant τ yielded a median relative standard deviation of 1.0 % (mean 1.3 %). This value is significantly smaller than the measurement uncertainty of the individual τ determinations, confirming that our MetDyHuCal procedure resolves genuine differences between sensors and is not influenced or limited by its own stability or repeatability.

Our static calibration results clearly demonstrate that individual sensor calibration is strongly advised for many LCrHS. All tested sensor models exhibit significant measurement offsets and slope deviations at a magnitude that renders uncalibrated use unsuitable for most applications that require accuracies better than 5 %. For several sensor models, including the AHT10 and the DHT22, the spread in offset values between individual sensors of the same model is so large that a generic, model-level correction would leave residual errors that substantially exceed the uncertainty of our static calibration. Furthermore, depending on the sensor model and the required measurement accuracy in the target application, a linear sensor model is not sufficient to describe the sensor response over the full operating range, so that at a 2nd or even 3rd-order polynomial correction is required.

Our dynamic characterisation results confirm that a 1st-order low-pass model is well suited to describe the response behaviour of all the evaluated LCrHS. However, several sensor models, most notably the HDC1080 and the HIH4000, show a strong systematic dependence of the characteristic time constant τ on the H_2O-level, so that a single τ value is insufficient to describe the dynamic behaviour of such sensors across their full H_2O operating range. In such cases, τ should be determined over the full H_2O range of the application with at least 3 H_2O levels if accurate dynamic correction is intended.

The comparison between the measured τ values and the manufacturer datasheets reveals large and unsystematic discrepancies, ranging from -50 % to +81 % relative to the manufacturer-specified values. These deviations arise from a combination of factors, including design differences in housing geometry, gas exchange characteristics, and in particular unclear calibration conditions and methods used by the manufacturers to determine the specified values. The lack of a defined, standardised and openly documented test procedure makes it impossible to compare the dynamic performance of sensors from different manufacturers on the basis of the datasheet information alone. Our results clearly demonstrate the need for a standardised approach to the dynamic characterisation of humidity sensors and in particular LCrHS.

Future work will focus on five areas. A) the placement of a second open-path dTDLAS measurement cell, directly behind the DUT mounting position in the flow channel. This addition instrument would allow to increase the accuracy of the two-dimensional fluid simulation and further reduce the uncertainty of the dynamic characterisation. B) the expansion of the characterization method to research instruments in combination with their respective gas sampling system. The need for such an investigation was already identified during the validation phase of the HAI instrument for the research aircraft HALO (Buchholz et al., 2017). C) the expansion of the dynH_2O setup to gases other than water vapour, enabling the dynamic characterisation of sensors for CO_2, CH_4, N_2O, NO_2, volatile organic compounds (VOCs), and other relevant atmospheric trace gases. D) the results of this work should contribute to ongoing national and international standardisation activities with the aim of establishing a harmonised dynamic test procedure for the characterisation of gas sensors and in particular hygrometers. E) More accurate and traceable H_2O line strengths. This would directly improve the accuracy of MANTA-LAH and SEALDH-II and could even improve our existing characterization data, by reevaluating the stored raw spectra of the two spectrometers.

https://doi.org/10.5194/egusphere-2026-6133
Preprint. Discussion started: 20 November 2026
© Author(s) 2026. CC BY 4.0 License.



Code and data availability

Due to the mentioned method of storing raw laser spectra at over 20 Hz (i.e. digitized photodetector currents vs. time) for the two laser instruments the size of the entire dataset is 227 GB. The size and high specificity of the dataset and the complex proprietary evaluation of the spectra makes a direct publication of our measurement data or an unsupported data evaluation unrealistic; the authors however are happy to cooperatively share and discuss useful subsets of the data upon request.

Author contributions

Conceptualization and design of the experiments by Volker Ebert (VE) and Felix Witt (FW). Funding and resource acquisition as well as project supervision was done by VE. Mechanical and electronic realization and automation of the dynH2O setup by FW. FW performed the measurements, data curation, formal analysis, validation and data visualisation. The used methodology and data evaluation software were developed by FW and VE. The original draft was written by FW and reviewed and edited by VE.

Competing interests

The authors declare that they have no conflict of interest.

Disclaimer

Copernicus Publications remains neutral with regard to jurisdictional claims made in the text, published maps, institutional affiliations, or any other geographical representation in this paper. While Copernicus Publications makes every effort to include appropriate place names, the final responsibility lies with the authors. Views expressed in the text are those of the authors and do not necessarily reflect the views of the publisher.

Acknowledgements

Special thanks to Mauritz Luszas for supporting the measurements in the lab and to Regina Deschermeier and Javis Nwaboh (PTB) for providing scientific equipment for the measurements.
The Scientific colour maps “batlow” and “bukavu” are used in this study to prevent visual distortion of the data and exclusion of readers with colour-vision deficiencies (Crameri et al., 2020).

Financial support

Part of the funding originates from the Deutsche Forschungsgemeinschaft (DFG) through the project HAI PolWise, project number 316868214. This work was also in part supported by the Physikalisch-Technische Bundesanstalt (PTB) the national metrology institute of Germany.

Review statement

The review statement will be added by Copernicus Publications listing the handling editor as well as all contributing referees according to their status anonymous or identified.

https://doi.org/10.5194/egusphere-2026-6133
Preprint. Discussion started: 20 November 2026
© Author(s) 2026. CC BY 4.0 License.

References

ASAIR: AHT10 Technical Manual V1.1, https://altronics.cl/uploads/AHT10.pdf, last access: 12 October 2026, 2018.

ASAIR: DHT22 AM2302 Technical Information, https://asairsensors.com/product/am2302-dht22-temperature-and-humidity-sensor/, last access: 23 September 2026.

Bärfuss, K., Pätzold, F., Altstädter, B., Kathe, E., Nowak, S., Bretschneider, L., Bestmann, U., and Lampert, A.: Correction: Bärfuss et al. New Setup of the UAS ALADINA for Measuring Boundary Layer Properties, Atmospheric Particles and Solar Radiation. (Atmosphere, 2018, 9, 28), Atmosphere 2018, 9(8), 306, https://doi.org/10.3390/atmos9080306, 2018.

Bärfuss, K. B., Schmithüsen, H., and Lampert, A.: Drone-based meteorological observations up to the tropopause – a concept study, Atmos. Meas. Tech., 16, 3739–3765, https://doi.org/10.5194/amt-16-3739-2023, 2023.

Bell, S., Stevens, M., Abe, H., Benyon, R., Bosma, R., Fernicola, V., Heinonen, M., Huang, P., Kitano, H., Li, Z., Nielsen, J., Ochi, N., Podmurnaya, O. A., Scace, G., Smorgon, D., Vicente, T., Vinge, A. F., Wang, L., and Yi, H.: Final report on CCT-K6: Comparison of local realisations of dew-point temperature scales in the range −50 °C to +20 °C, Metrologia, 52, 3005, https://doi.org/10.1088/0026-1394/52/1A/03005, 2015.

BIPM: JCGM 100:2008: Evaluation of measurement data - Guide to the expression of uncertainty in measurement, Bureau International des poids et Mesures, https://doi.org/10.59161/JCGM100-2008E, 2008.

BIPM: Key Comparison Database, Bureau International des Poids et Mesures, https://www.bipm.org/kcdb/, last access: 23 September 2026.

Bosch: BME280 - Data sheet: BST-BME280-DS001-24, https://www.bosch-sensortec.com/en/products/environmental-sensors/humidity-sensors-bme280, last access: 12 October 2026, 2024.

Buchholz, B. and Ebert, V.: Offsets in fiber-coupled diode laser hygrometers caused by parasitic absorption effects and their prevention, Meas. Sci. Technol., 25, 75501, https://doi.org/10.1088/0957-0233/25/7/075501, 2014.

Buchholz, B., Böse, N., and Ebert, V.: Absolute validation of a diode laser hygrometer via intercomparison with the German national primary water vapor standard, Appl. Phys. B, 116, 883–899, https://doi.org/10.1007/s00340-014-5775-4, 2014.

Buchholz, B., Afchine, A., Klein, A., Schiller, C., Krämer, M., and Ebert, V.: HAI, a new airborne, absolute, twin dual-channel, multi-phase TDLAS-hygrometer: background, design, setup, and first flight data, Atmos. Meas. Tech., 10, 35–57, https://doi.org/10.5194/amt-10-35-2017, 2017.

Buchholz, B., Kallweit, S., and Ebert, V.: SEALDH-II-An Autonomous, Holistically Controlled, First Principles TDLAS Hygrometer for Field and Airborne Applications: Design-Setup-Accuracy/Stability Stress Test, MDPI Sensors (Basel, Switzerland), 68, https://doi.org/10.3390/s17010068, 2016.

Crameri, F., Shephard, G. E., and Heron, P. J.: The misuse of colour in science communication, Nature communications, 11, 5444, https://doi.org/10.1038/s41467-020-19160-7, 2020.

E+E Elektronik GmbH: Datasheet HTE301: Digital Humidity and Temperature Sensor, https://www.epluse.com/de/produkte/feuchtemesstechnik/digitale-feuchtesensorelemente/hte301/#product_downloads, last access: 23 September 2026, 2023a.

E+E Elektronik GmbH: Datasheet HTE501: Digital Humidity and Temperature Sensor, https://www.epluse.com/de/produkte/feuchtemesstechnik/digitale-feuchtesensorelemente/hte501/#product_downloads, last access: 23 September 2026, 2023b.

E+E Elektronik GmbH: Humidity Measurement in Fuel Cells, https://www.epluse.com/news/blog/detail/2023-03-17-humidity-measurement-in-fuel-cells/, last access: 10 April 2026, 2022.

Ebert, V.: In situ Absorption Spectrometers Using Near-IR Diode Lasers and Rugged Multi-Path-Optics for Environmental Field Measurements, Laser Applications to Chemical, Security and Environmental Analysis, Technical Digest (Optica Publishing Group, 2006), WB1, https://doi.org/10.1364/LACSEA.2006.WB1, 2006.

https://doi.org/10.5194/egusphere-2026-6133
Preprint. Discussion started: 20 November 2026
© Author(s) 2026. CC BY 4.0 License.



Ebert, V. and Wolfrum, J.: Absorption, in: Optical Measurements: Techniques and Applications, 2nd ed., edited by: Mayinger, F. and Feldmann, O., Springer, Berlin, Heidelberg, 231–270, https://doi.org/10.1007/978-3-642-56443-7_13, 2001.

Fernicola, V., Beltramino, G., Castrillo, A., Cuccaro, R., Deschermeier, R., Ebert, V., Enescu, D., Gianfrani, L., Gliese, P. J., Gravina, S., Hudoklin, D., Nobakht, R., Radičević, I., Rosso, L., and Tabandeh, S.: Primary Humidity Standards for Trace Water Measurements in Ultra-High-Purity Process Gases, MDPI Sensors (Basel, Switzerland), 26(13), 4222, https://doi.org/10.3390/s26134222, 2026.

Gordon, I. E., Rothman, L. S., Hargreaves, R. J., Gomez, F. M., Bertin, T., Hill, C., Kochanov, R. V., Tan, Y., Wcisło, P., Makhnev, V. Y., Bernath, P. F., Birk, M., Boudon, V., Campargue, A., Coustenis, A., Drouin, B. J., Gamache, R. R., Hodges, J. T., Jacquemart, D., Mlawer, E. J., Nikitin, A. V., Perevalov, V. I., Rotger, M., Robert, S., Tennyson, J., Toon, G. C., Tran, H., Tyuterev, V. G., Adkins, E. M., Barbe, A., Bailey, D. M., Bielska, K., Bizzocchi, L., Blake, T. A., Bowesman, C. A., Cacciani, P., Čermák, P., Császár, A. G., Denis, L., Egbert, S. C., Egorov, O., Ermilov, A. Y., Fleisher, A. J., Fleurbaey, H., Foltynowicz, A., Furtenbacher, T., Germann, M., Guest, E. R., Harrison, J. J., Hartmann, J.-M., Hjältén, A., Hu, S.-M., Huang, X., Johnson, T. J., Jóźwiak, H., Kassi, S., Khan, M. V., Kwabia-Tchana, F., Lee, T. J., Lisak, D., Liu, A.-W., Lyulin, O. M., Malarich, N. A., Manceron, L., Marinina, A. A., Massie, S. T., Mascio, J., Medvedev, E. S., Meshkov, V. V., Mellau, G. C., Melosso, M., Mikhailenko, S. N., Mondelain, D., Müller, H., O'Donnell, M., Owens, A., Perrin, A., Polyansky, O. L., Raston, P. L., Reed, Z. D., Rey, M., Richard, C., Rieker, G. B., Röske, C., Sharpe, S. W., Starikova, E., Stolarczyk, N., Stolyarov, A. V., Sung, K., Tamassia, F., Terragni, J., Ushakov, V. G., Vasilchenko, S., Vispoel, B., Vodopyanov, K. L., Wagner, G., Wójtewicz, S., Yurchenko, S. N., and Zobov, N. F.: The HITRAN2024 molecular spectroscopic database, Journal of Quantitative Spectroscopy and Radiative Transfer, 353, 109807, https://doi.org/10.1016/j.jqsrt.2026.109807, 2026.

Greenspan, L.: Functional Equations for the Enhancement Factors for CO2-Free Moist Air, Journal of research of the National Bureau of Standards. Section A, Physics and chemistry, 80A, 41–44, https://doi.org/10.6028/jres.080A.007, 1976.

Gupta, N., Pathania, P., Goel, K., Sharma, T., and Deb, S.: Open Source SoC Design for Low-Cost Micro Weather Station, in: 2024 IEEE International Symposium on Smart Electronic Systems (iSES), New Delhi, India, 16-18 December 2024, 173–176, https://doi.org/10.1109/iSES63344.2024.00043, 2024.

Hartono, J. R. and Utama, D. N.: Monitoring the Effectiveness of Energy Consumption for Old Buildings Using Data Gathered Through Temperature, Humidity, and Light Intensity, jppipa, pendidikan ipa, fisika, biologi, kimia, 11, 149–159, https://doi.org/10.29303/jppipa.v11i12.11706, 2025.

Heinonen, M., Cavallarin, L., Dell'Isola, M., Ebert, V., Fernicola, V., Georgin, E., Hudoklin, D., Nielsen, J., Østergaard, P. F., Peruzzi, A., Pietari, T., Wagner, S., and Werhahn, O.: Metrology for humidity at high temperatures and transient conditions, in: 17th International Congress of Metrology, Paris, France, September 21-24, 2015, 15015, https://doi.org/10.1051/metrology/20150015015, 2015.

Holovatyy, A.: Development of IoT Weather Monitoring System Based on Arduino and ESP8266 Wi-Fi Module, IOP Conf. Ser.: Mater. Sci. Eng., 1016, 12014, https://doi.org/10.1088/1757-899X/1016/1/012014, 2021.

Honeywell International Inc.: HIH-4000 Series Humidity Sensors, https://prod-edam.honeywell.com/content/dam/honeywell-edam/sps/siot/de-de/products/sensors/humidity-with-temperature-sensors/hih-4000-series/documents/sps-siot-hih4000-series-product-sheet-009017-5-en-ciid-49922.pdf, last access: 23 September 2026, 2010.

Hooshmand, A. H.: Smart modular greenhouse control via IoT, LabVIEW, and PSO-PID integration, Computers and Electrical Engineering, 128, 110713, https://doi.org/10.1016/j.compeleceng.2025.110713, 2025.

Hossain, F. M., Tan, D. J. G., Ameer, I. M., Ayun, Q. Q., Matsunaga, S., Junaideen, S. A., and Liang, Z.: From Skin to Screen: Real-Time Wound Monitoring with a Smart Bandage and Smartphone, in: 2025 IEEE 14th Global Conference on Consumer Electronics (GCCE), Osaka, Japan, 23-26 September 2025, 712–714, https://doi.org/10.1109/GCCE65946.2025.11275449, 2025.

https://doi.org/10.5194/egusphere-2026-6133
Preprint. Discussion started: 20 November 2026
© Author(s) 2026. CC BY 4.0 License.

Hunsmann, S., Wagner, S., Saathoff, H., Möhler, O., Schurath, U., and Ebert, V.: Messung der Temperaturabhängigkeit der Linienstärken und Druckverbreiterungskoeffizienten von H2O-Absorptionslinien im 1.4µm-Band, VDI-Berichte, 1959, 149–164, available at: http://tubiblio.ulb.tu-darmstadt.de/52530/, 2006.

Koestoer, R. A., Pancasaputra, N., Roihan, I., and Harinaldi: A simple calibration methods of relative humidity sensor DHT22 for tropical climates based on Arduino data acquisition system, in: AIP Conference Proceedings 2062, Bali, Indonesia, 16–17 November 2018, 020009, https://doi.org/10.1063/1.5086556, 2019.

Liptak, B.: Instrument Engineers' Handbook: Process Control and Optimization, 4th ed., 2, CRC Press, Boca Raton, https://doi.org/10.1201/9781420064001, 2005.

Macagga, R., Asante, M., Sossa, G., Antonijević, D., Dubbert, M., and Hoffmann, M.: Validation and field application of a low-cost device to measure CO 2 and evapotranspiration (ET) fluxes, Atmos. Meas. Tech., 17, 1317–1332, https://doi.org/10.5194/amt-17-1317-2024, 2024.

Manninen, A., Tuzson, B., Looser, H., Bonetti, Y., and Emmenegger, L.: Versatile multipass cell for laser spectroscopic trace gas analysis, Appl. Phys. B, 109, 461–466, https://doi.org/10.1007/s00340-012-4964-2, 2012.

Markwitz, C. and Siebicke, L.: Low-cost eddy covariance: a case study of evapotranspiration over agroforestry in Germany, Atmos. Meas. Tech., 12, 4677–4696, https://doi.org/10.5194/amt-12-4677-2019, 2019.

Merlone, A., Sanna, F., Beges, G., Bell, S., Beltramino, G., Bojkovski, J., Brunet, M., Del Campo, D., Castrillo, A., Chiodo, N., Colli, M., Coppa, G., Cuccaro, R., Dobre, M., Drnovsek, J., Ebert, V., Fernicola, V., Garcia-Benadí, A., Garcia-Izquierdo, C., Gardiner, T., Georgin, E., Gonzalez, A., Groselj, D., Heinonen, M., Hernandez, S., Högström, R., Hudoklin, D., Kalemci, M., Kowal, A., Lanza, L., Miao, P., Musacchio, C., Nielsen, J., Nogueras-Cervera, M., Oguz Aytekin, S., Pavlasek, P., Podesta, M. de, Rasmussen, M. K., del-Río-Fernández, J., Rosso, L., Sairanen, H., Salminen, J., Sestan, D., Šindelářová, L., Smorgon, D., Sparasci, F., Strnad, R., Underwood, R., Uytun, A., and Voldan, M.: The MeteoMet2 project—highlights and results, Meas. Sci. Technol., 29, 25802, https://doi.org/10.1088/1361-6501/aa99fc, 2018.

Mihajlo, K., Luka, G., Nikola, N., and Vladimir, R.: Design of stored grain monitoring system based on NB-IoT, in: 2020 28th Telecommunications Forum (TELFOR), Belgrade, Serbia, 24-25 November 2020, 1–4, https://doi.org/10.1109/TELFOR51502.2020.9306646, 2020.

Mitter, H.: Feuchte-Ansprechverhalten von kapazitiven Polymersensoren bei tiefen Temperaturen: Humidity Response Time of Capacitive Polymer Sensors at Low Temperatures, in: Proceedings Temperatur 2026: Fachtagung Physikalisch-Technische Bundesanstalt, Berlin, Germany, 16.-17. Mai, 225–232, available at: https://www.researchgate.net/publication/286876610_Feuchte-Ansprechverhalten_von_kapazitiven_Polymersensoren_bei_tiefen_Temperaturen_Humidity_Response_Time_of_Capacitive_Polymer_Sensors_at_Low_Temperatures, last access: 12 October 2026, 2006.

NF X 15-113: Measurement of Air Humidity - Impedance Variation Hygrometer (Capacitive and Resistance), Association Francaise de Normalisation, 1997.

Nielsen, L.: Evaluation of measurements by the method of least squares, in: Algorithms For Approximation IV: Proceedings of the 2001 International Symposium, University of Huddersfield, 16 - 20 July 2021, 170–186, available at: https://www.researchgate.net/publication/235212639_Evaluation_of_Measurements_by_the_Method_of_Least_Squares, last access: 12 October 2026, 2002.

Nikolaev, D. V., Popov, V. I., Timofeev, V. B., and Smagulova, S. A.: Chemical Vapor Deposition Synthesis of Large-Area Graphene Films, J Struct Chem, 59, 766–772, https://doi.org/10.1134/S0022476618040030, 2018.

Nwaboh, J. A., Werhahn, O., and Ebert, V.: H2O Collisional Broadening Coefficients at 1.37 µm and Their Temperature Dependence: A Metrology Approach, Applied Sciences, 11, 5341, https://doi.org/10.3390/app11125341, 2021a.

Nwaboh, J. A., Qu, Z., Werhahn, O., and Ebert, V.: Towards an Optical Gas Standard for Traceable Calibration-Free and Direct NO2 Concentration Measurements, Applied Sciences, 11, 5361, https://doi.org/10.3390/app11125361, 2021b.

https://doi.org/10.5194/egusphere-2026-6133
Preprint. Discussion started: 20 November 2026
© Author(s) 2026. CC BY 4.0 License.

Pogány, A., Klein, A., and Ebert, V.: Measurement of water vapor line strengths in the 1.4–2.7 µm range by tunable diode laser absorption spectroscopy, Journal of Quantitative Spectroscopy and Radiative Transfer, 165, 108–122, https://doi.org/10.1016/j.jqsrt.2015.06.023, 2015.

Santos Jr, J. L., Silva, L. H. P., Andrade, I. R., Rosa, R., and Abegão, L. M. G.: Real-world deployment of an affordable sub-soil temperature and relative humidity sensing system for precision agriculture, Meas. Sci. Technol., 36, 115113, https://doi.org/10.1088/1361-6501/ae1c63, 2025.

Sari, I. P., Gunawan, A. A. N., Wibawa, I. M. S., Putra, I. K., and Yusuf, M.: Design of Radiosonde Based on Arduino Pro Mini Using BME280 Sensor, in: Techniques and Innovation in Engineering Research Vol. 5, edited by: Sheu, D. G. Y., B P International (a part of SCIENCEDOMAIN International), 145–157, https://doi.org/10.9734/bpi/taier/v5/18576D, 2023.

Sensirion: Datasheet SHT3x-DIS: Humidity and Temperature Sensor, V. 7, https://sensirion.com/products/catalog/SHT31-DIS-B, last access: 12 October 2026, 2022.

Sonntag, D.: Important New Values of the Physical Constants of 1986, Vapour Pressure Formulations Based on the ITS-90, and Psychrometer Formulae, Zeitschrift für Meteorologie, 340–344, 1990.

TE Connectivity: HTU21D(F) RH/T SENSOR IC: Digital Relative Humidity sensor with Temperature output, https://www.te.com/de/product-CAT-HSC0004.html, last access: 23 September 2026, 2017.

Texas Instruments: HDC1080 Low Power, High Accuracy Digital Humidity Sensor with Temperature Sensor, https://www.ti.com/document-viewer/HDC1080/datasheet, last access: 12 October 2026, 2016.

Tuma, D.: Final Publishable Report: Metrology for Hydrogen Storage Solutions (MefHySto, 19ENG03), EURAMET, https://www.euramet.org/research-innovation/search-research-projects/details/?tx_eurametctcp_project[project]=1681, last access: 12 October 2026, 2023.

Tuzson, B., Mangold, M., Looser, H., Manninen, A., and Emmenegger, L.: Compact multipass optical cell for laser spectroscopy, Opt. Lett., OL, 38, 257–259, https://doi.org/10.1364/OL.38.000257, 2013.

VDI/VDE 3514 Blatt 3: Measurement of humidity - Calibration and measurement uncertainty, VDI, available at: https://www.vdi.de/mitgliedschaft/vdi-richtlinien/details/vdivde-3514-blatt-3-gasfeuchtemessung-kalibrierung-und-messunsicherheit, last access: 12 October 2026, 2021.

Wang, F., Lou, W. Z., Guo, M. R., and Lu, Y. F.: Intelligent Logistics Monitoring Microsystem Based on STM32, Key Engineering Materials (KEM), 645-646, 896–899, https://doi.org/10.4028/www.scientific.net/KEM.645-646.896, 2015.

Wang, L.: From Plant Data to Process Control: Ideas for Process Identification and PID Design, Taylor and Francis, Hoboken, 239 pp., https://doi.org/1201/9781482273007, 2014.

Wettstein, S. and Mutter, D.: Design and Validation of the MBW Standard Humidity Generators, Int J Thermophys, 39, https://doi.org/10.1007/s10765-018-2436-6, 2018.

Witt, F., Bubser, F., Ebert, V., and Bergmann, D.: C9.1 Temporal Hygrometer Characterization: Design and First Test of a New, Metrological Dynamic Testing Infrastructure, in: System of Units and Metreological Infrastructure: Proceedings of SMSI 2021, digital, 5/3/2021 - 5/6/2021, 308–309, https://doi.org/10.5162/SMSI2021/C9.1, 2021a.

Witt, F. and Ebert, V.: dynH2O: A Metrological Approach to Manage the Effects of Dynamic H2O Concentration Changes on Hygrometers in the Field, in: Proceedings EGU General Assembly 2023, Vienna, 24–28 Apr, EGU23-17526, https://doi.org/10.5194/egusphere-egu23-17526, 2023.

Witt, F., Bohlius, H., and Ebert, V.: Evaluation of Spatial Gas Temperature and Water Vapor Inhomogeneities in TDLAS in Circular Multipass Absorption Cells Used for the Analysis of Dynamic Tube Flows, MDPI Sensors (Basel, Switzerland), 23, https://doi.org/10.3390/s23094345, 2023a.

Witt, F., Schuchard, M., and Ebert, V.: DynH2O Aufbau zur metrologischen Charakterisierung der dynamischen Eigenschaften von Hygrometern, tm - Technisches Messen, 90, 79–89, https://doi.org/10.1515/teme-2021-0144, 2023b.

https://doi.org/10.5194/egusphere-2026-6133
Preprint. Discussion started: 20 November 2026
© Author(s) 2026. CC BY 4.0 License.



Witt, F., Nwaboh, J., Bohlius, H., Lampert, A., and Ebert, V.: Towards a Fast, Open-Path Laser Hygrometer for Airborne Eddy Covariance Measurements, Applied Sciences, 11, 5189, https://doi.org/10.3390/app11115189, 2021b.

Wiyagi, R. O., Danardono, D., and Try, A. A.: High Altitude Balloon Payload Design for Atmospheric Observations, Journal of Electrical Technology UMY (jet), 1, https://doi.org/10.18196/jet.1107, 2017.

Zhang, M., Sun, H., Li, M., and Zheng, L.: Development of a new type monitoring system of leaf surface temperature and humidity, in: ASABE Annual International Meeting 2014, July 13-16 2014, 1–8, https://doi.org/10.13031/aim.20141897244, 2014.